

Experimental methods in astroparticle physics

SS2020

Teresa Marrodán Undagoitia

Max-Planck-Institut für Kernphysik,
Saupfercheckweg 1, 69117 Heidelberg, Germany

E-mail: marrodan@mpi-hd.mpg.de

Contents

1	Lecture 4: Direct detection of dark matter	2
1.1	Dark matter signatures	2
1.2	Cross sections for scattering on nucleons and form factors	4
1.3	Generic result of a dark matter experiment	6
1.4	Background in direct detection	7
1.5	Statistical treatment of data	12
1.6	Detector calibration	13
1.7	Technologies and results	13
	1.7.1 Scintillation detectors	14
	1.7.2 Cryogenic bolometers	15
	1.7.3 Liquid noble-gas detectors	16
	1.7.4 Bubble chambers	18
	1.7.5 Directional searches	18
1.8	Summary	20

1. Lecture 4: Direct detection of dark matter

In this lecture, we discuss the direct detection of dark matter. Dark matter particles orbiting in the gravitational potential of the Milky Way can elastically interact with target nuclei in a detector medium. A variety of technologies have been developed and detectors are constructed to eventually catch these rare nuclear recoils. We will discuss all relevant aspects related to direct detection and different detector concepts. Note that here we are focussing on WIMPs scattering off nuclei but certain dark matter candidates could, in principle, interact off shell electrons.

1.1. Dark matter signatures

The most common approach in direct detection experiments is the attempt to measure the energy dependence of dark matter interactions. For a $(10-100) \text{ GeV}/c^2$ WIMP mass with velocities as expected from the Milky Way standard halo model, nuclear recoils of $(1-100) \text{ keV}$ result. The differential recoil spectrum resulting from dark matter interactions can be written [1] as

$$\frac{dR}{dE}(E, t) = \frac{\rho_0}{m_\chi \cdot m_A} \cdot \int v \cdot f(\mathbf{v}, t) \cdot \frac{d\sigma}{dE}(E, v) d^3v, \quad (1)$$

where m_χ is the dark matter mass and $\frac{d\sigma}{dE}(E, v)$ its differential cross-section. The WIMP cross-section σ and m_χ are the two observables of a dark matter experiment. The dark matter velocity v is defined in the rest frame of the detector and m_A is the nucleus mass. Equation 1 shows explicitly the astrophysical parameters, the local dark matter density ρ_0 and $f(\mathbf{v}, t)$, which accounts for the WIMP velocity distribution in the detector reference frame. According to [1], equation 1 can be approximated by

$$\frac{dR}{dE}(E) \approx \left(\frac{dR}{dE}\right)_0 F^2(E) \exp\left(-\frac{E}{E_c}\right), \quad (2)$$

where $\left(\frac{dR}{dE}\right)_0$ denotes the event rate at zero momentum transfer and E_c is a constant parameterizing a characteristic energy scale which depends on the dark matter mass and target nucleus. Hence, the signal is dominated at low recoil energies by the exponential function. $F^2(E)$ is the form-factor correction which will be described later.

Exercise related to event rates

Another possible dark matter signature is the so-called 'annual modulation'. As a consequence of the Earth rotation around the Sun, the speed of the dark matter particles in the Milky Way halo relative to the Earth is largest around June 2nd and smallest in December (see figure 1). Consequently, the amount of particles able to produce nuclear recoils above the detectors' energy threshold is also largest in June [2]. As the amplitude of the variation is expected to be small, the temporal variation of the differential event rate can be written following [3] as

$$\frac{dR}{dE}(E, t) \approx S_0(E) + S_m(E) \cdot \cos\left(\frac{2\pi(t - t_0)}{T}\right), \quad (3)$$

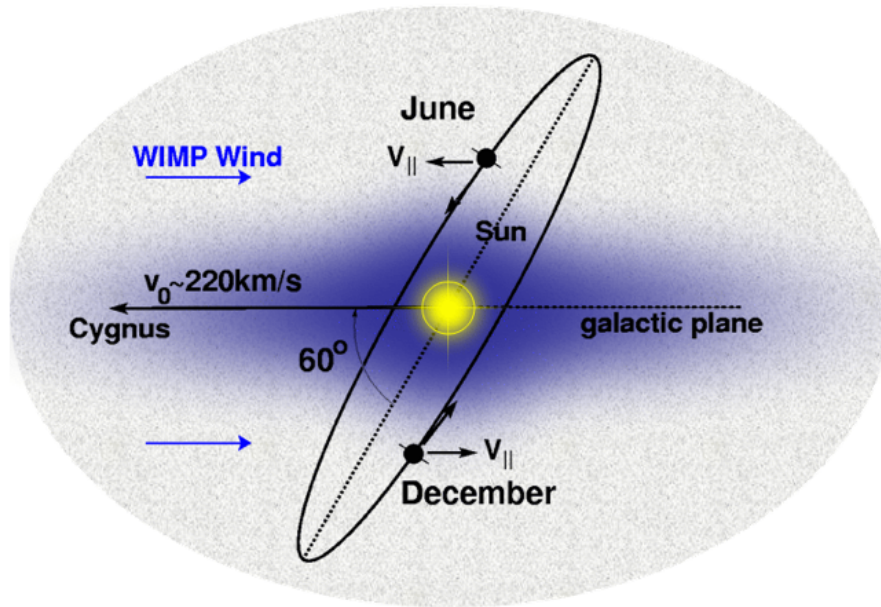


Figure 1. Scheme of the relative movement of the Earth and WIMPs that give an annual modulation of the dark matter rate.

where t_0 is the phase which is expected at about 150 days and T is the expected period of one year. The time-averaged event rate is denoted by S_0 , whereas the modulation amplitude is given by S_m . The rate modulation would, in principle, enhance the ability to discriminate against background and help to confirm a dark matter detection.

Directionality is another dark-matter signature which can be employed for detection as the direction of the nuclear recoils resulting from WIMP interactions has a strong angular dependence [4]. This dependence can be seen in the differential rate equation when it is explicitly written as a function of the angle γ , defined by the direction of the nuclear recoil relative to the mean direction of the solar motion

$$\frac{dR}{dE d\cos\gamma} \propto \exp\left[\frac{-[(v_E + v_\odot)\cos\gamma - v_{min}]^2}{v_c^2}\right]. \quad (4)$$

In equation 4, v_E represents the Earth's motion, v_\odot the velocity of the Sun around the galactic centre, v_{min} the minimum WIMP velocity that can produce a nuclear recoil of an energy E and v_c the halo circular velocity $v_c = \sqrt{3/2}v_\odot$. The rate of events scattering in the forward direction will, therefore, exceed the rate for backwards scattering events. A detector able to determine the direction of the WIMP-induced nuclear recoil would provide a powerful tool to confirm the measurement of these particles.

Figure 2 shows the directionally signature of a dark matter signal. While the uppermost panel shows the flux of WIMP particles, the middle panel accounts for the directional smearing due to the recoiling process. The bottom panel shows a simulated example with 100 WIMP particles and 100 background events.

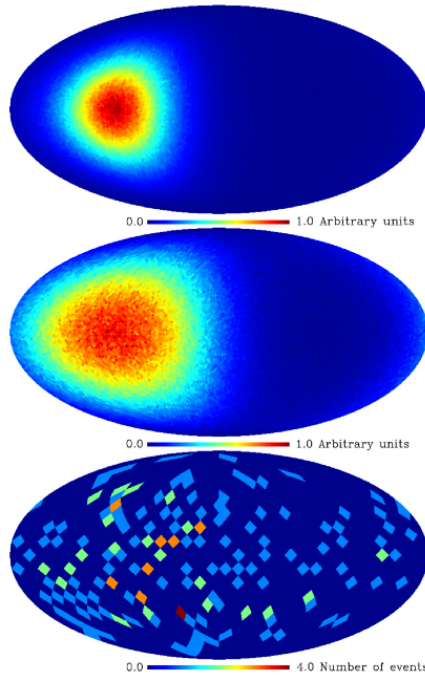


Figure 2. Directionality signature: (top) WIMP flux in the case of an isothermal spherical halo, (middle) WIMP-induced recoil distribution and (bottom) a typical simulated measurement: 100 WIMP recoils and 100 background events (low angular resolution). Figure from J. Billard et al. 2010.

1.2. Cross sections for scattering on nucleons and form factors

Typically, two cases are considered for the cross section of dark matter particles with ordinary matter: spin-independent and dependent. For interactions that are independent of spin, it is assumed that neutrons and protons contribute equally to the scattering process (isospin conservation). For sufficiently low momentum transfer q , the amplitudes of the scattering off each nucleon add in phase and result in a coherent process. For spin-dependent interactions, only unpaired nucleons contribute to the scattering process. For this reason, only nuclei with an odd number of protons or neutrons are sensitive to these interactions. In this case, the cross-section is related to the quark spin content of the nucleon with components from both proton and neutron couplings.

When the momentum transfer is such that the particle wavelength is no longer large compared to the nuclear radius, the cross-section decreases with increasing q . The form factor F accounts for this effect and the cross-section can be expressed as:

$$\sigma \propto \sigma_0 \cdot F^2 \tag{5}$$

where σ_0 is the cross-section at zero momentum transfer.

The differential WIMP-nucleus cross section, $d\sigma/dE$ shown in equation 1, can be written in general as the sum of a spin-independent (SI) contribution and a spin-

dependent (SD) one,

$$\frac{d\sigma}{dE} = \frac{m_A}{2\mu_A^2 v^2} \cdot (\sigma_0^{\text{SI}} \cdot F_{\text{SI}}^2(E) + \sigma_0^{\text{SD}} \cdot F_{\text{SD}}^2(E)). \quad (6)$$

The WIMP-nucleus reduced mass is described by μ_A . For spin independent interactions, the cross-section at zero momentum transfer can be expressed as

$$\sigma_0^{\text{SI}} = \sigma_p \cdot \frac{\mu_A^2}{\mu_p^2} \cdot [Z \cdot f^p + (A - Z) \cdot f^n]^2 \quad (7)$$

where $f^{p,n}$ are the contributions of protons and neutrons to the total coupling strength, respectively, and μ_p is the WIMP-nucleon reduced mass. Usually, $f^p = f^n$ is assumed and the dependence of the cross-section with the number of nucleons A takes an A^2 form. The form factor for SI interactions is calculated assuming the distribution of scattering centres to be the same as the charge distribution derived from electron scattering experiments [1]. Commonly, the Helm parameterisation [5] is used to describe the form factor.

Figure 3 (left) shows the event rate given in number of events per keV, day and kg (equation 1) for spin-independent interactions in different target materials: tungsten in green, xenon in black, iodine in magenta, germanium in red, argon in blue and sodium in grey. A WIMP mass of $100 \text{ GeV}/c^2$ and a cross-section of 10^{-45} cm^2 are assumed for the calculation.

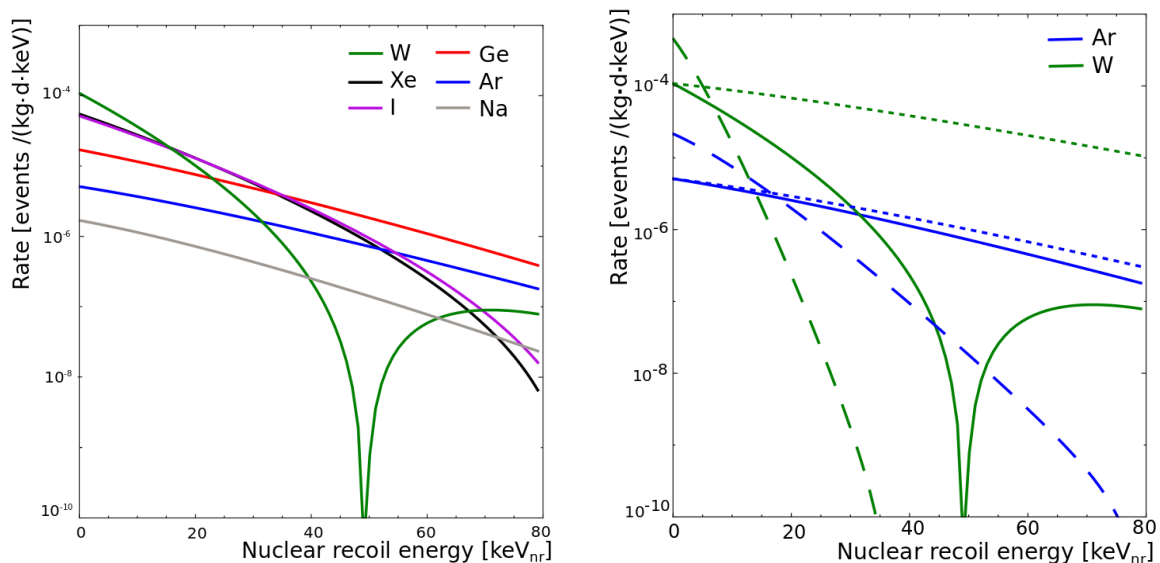


Figure 3. (Left) Event rates as function of nuclear recoil energy for different target materials assuming a $100 \text{ GeV}/c^2$ WIMP mass and an interaction cross section of 10^{-45} cm^2 (solid lines). (Right) Event rates for argon and tungsten. Dotted line: no form factor correction. Dashed line: for a $25 \text{ GeV}/c^2$ WIMP mass. Figures from [6].

In these curves, the shape of the energy spectrum is affected by both the A^2 dependence of the cross-section and the form factor correction. Heavier elements profit

from the A^2 enhancement with a higher event rate at low deposited energies but the coherence loss due to the form factor suppresses the event rate especially at higher recoil energies. Therefore, for lighter targets a low energy threshold is of less relevance than for the heavier ones.

Figure 3 (right) shows separately the WIMP mass and the form factor effect on the differential event rate without considering the nuclear recoil acceptance and the energy threshold of the detector. Solid lines show the expected rates for a $100 \text{ GeV}/c^2$ WIMP as in the left figure for a heavy and a light target as indicated in green (tungsten) and blue (argon), respectively. In comparison to the heavy WIMP mass the rates for a $25 \text{ GeV}/c^2$ dark matter particle (dashed line) drop steeper as the momentum transfer is smaller. The form factor correction for a heavy target is more important than for light targets. This can be seen by the dotted lines representing rates for a $100 \text{ GeV}/c^2$ WIMP, calculated without the form factor correction.

1.3. Generic result of a dark matter experiment

Outcome of an experiment is an event rate with a certain spectral shape. Due to the low cross section expected for dark matter particles, a single interaction is expected. Besides the signal signatures discussed earlier, there are a few characteristic features:

- Single scattering: by rejecting multiple simultaneous interactions, the background from environmental radioactivity can be suppressed.
- Spatial distribution: while the dark matter interactions are expected to be homogeneously distributed in space, background is more likely at large radii. For this reason an innermost volume, called fiducial volume, is typically selected to further mitigate backgrounds.

The results of a direct detection experiment are commonly displayed in a parameter space of the dark matter-nucleon cross-section and the dark matter mass. If there is statistical significance of signal over the expected background, signal contours at a certain confidence level (2σ are typical). If there isn't, a curve as the left plot in figure 4, generic limit (open black curve). At low WIMP masses the sensitivity is reduced mainly due to the low-energy threshold of the detector. The minimum of the exclusion curve is given by the kinematics of the scattering process which depends on the target nucleus mass. At large WIMP masses, the event rate is overall suppressed by $1/m_\chi$.

Figure 4 (right panel) shows the evolution of the sensitivity to the cross-section versus the exposure. For a given detector mass, the increase in exposure is caused by the accumulation of measuring time.

[Exercise about this topic](#)

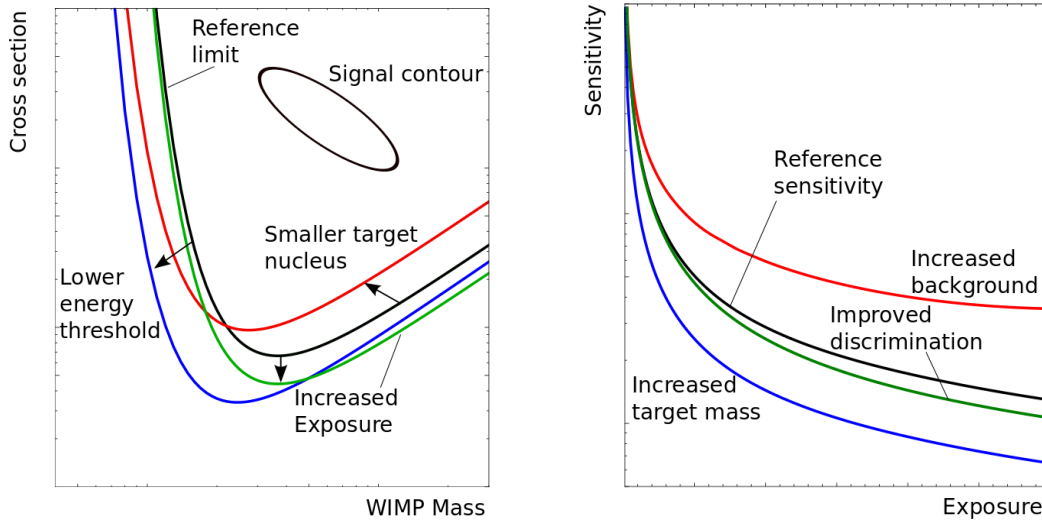


Figure 4. Sensitivity of direct detection experiments. Figures from [6].

1.4. Background in direct detection

Events from dark matter interactions with ordinary matter are, if measured, extremely rare. For this reason, a great experimental effort is devoted to understand and suppress experimental backgrounds. This section reviews background sources and measures to mitigate backgrounds.

Gamma radiation

The dominant contribution from gamma-radiation originates from the decays in the natural uranium and thorium chains, as well as from decays of common isotopes as ^{40}K , ^{60}Co and ^{137}Cs present in the surrounding materials. The corresponding energy deposited in a detector ranges from keV up to 2.6 MeV (highest γ -energy from the thorium chain). The interactions of γ -rays with matter include the photoelectric effect, Compton scattering and $e^- e^+$ pair production [7]. In all these processes, an electron (or electron and positron for the pair production) is emitted which can contribute to the experiment's background. There several strategies to suppress gamma activity:

- Selecting materials with low radioactive traces: Gamma-spectroscopy using high-purity germanium detectors is a common technique to screen and select radio-pure materials. Alternatively, mass spectrometry or neutron activation analysis can be conducted.
- Shielding: surrounding the detector by a material with a high atomic number and a high density, i.e. good stopping power, and low internal contamination. Lead is a common material (see figure 5) but also large water tanks are employed: homogeneous shielding and low background.

[Exercise about shielding](#)

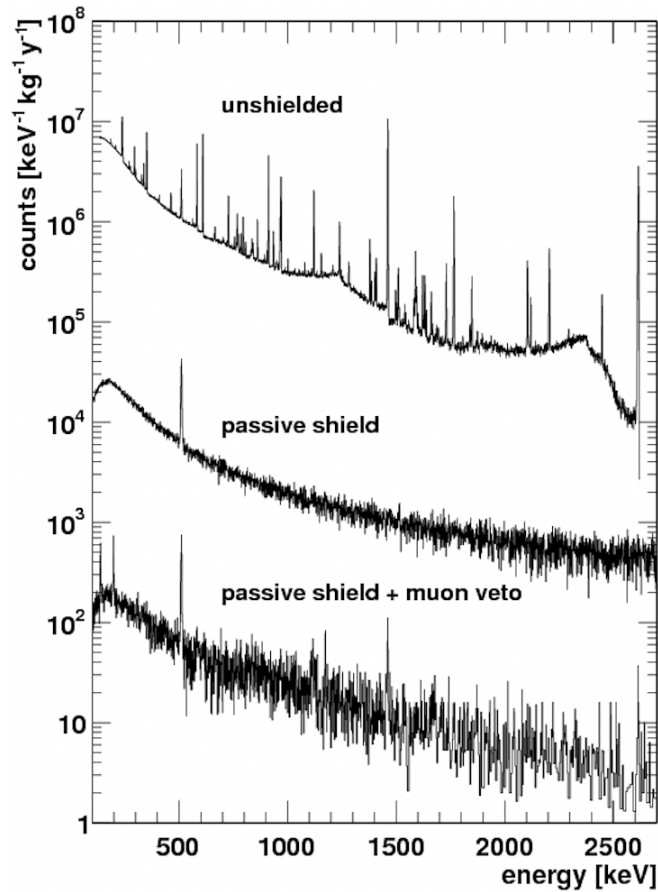


Figure 5. Spectral background comparison of the GIOVE germanium detector (at the shallow underground lab at MPIK) for increasing measures of passive (lead) and active shield (lead + scintillation muon panels). Figure from [8].

Neutron radiation

Neutrons can interact with target nuclei via elastic scattering producing nuclear recoils. This is one of the most dangerous background as it leaves a signal identical to the one of the WIMPs. Neutrons are generally separated into two types:

- Cosmogenic neutrons: originating from spallation reactions of muons on nuclei in the experimental setup or surrounding rock. Neutron energies up to several GeV which are moderated to MeV energies \rightarrow can produce nuclear recoils in the energy regime relevant for dark matter searches.
- Radiogenic neutrons: emitted in (α, n) - and spontaneous fission reactions from natural radioactivity (MeV energies)

To minimize cosmogenic neutrons, the experiments are typically placed at underground laboratories. The deeper the location of the laboratory, the lower the muon flux. Figure 5 shows the muon flux as a function of depth for different underground laboratories. The x-axis is given in km water equivalent, this quantity has to be multiplied by the density of the rock to obtain the value in km.

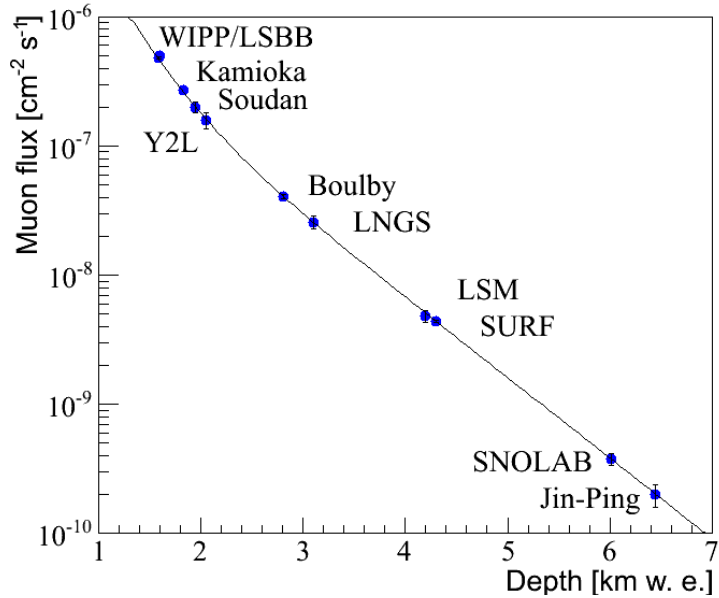


Figure 6. Muon flux measured for the various underground sites as function of the equivalent vertical depth. Figure from [6].

The contribution from radiogenic neutrons can also be reduced by different means. Also in this case, materials with low uranium and thorium content can be selected as they give lower α - and spontaneous fission rates. In addition, neutrons can be shielded/moderated by surrounding the detector with water or polyethylene layers. Figure 7 shows three examples of detector shielding. Active vetoes are designed to



Figure 7. Examples of detector shielding: DAMA detector (left), XENON100 detector (middle) and XENON1T water tank (right). Figures from the corresponding collaborations.

record interactions of muons. Plastic scintillator plates are, for example, used for this purpose. For large detectors large water Cherenkov detectors are employed, they provide a higher muon tagging efficiency (full coverage) and are efficient in stopping neutrons and external gammas. To tag directly the interactions of neutrons, liquid scintillator shielding detectors are used.

Neutrino background

With increasing target masses (hundreds of kilograms to tons) dark-matter detectors become sensitive to neutrino interactions both with electrons and with nuclei. Neutrinos can scatter elastically with electrons in the target via charged and/or neutral current interactions producing electronic recoils [9]. The most important source of neutrinos is the Sun: pp- and ${}^7\text{Be}$ -neutrinos (large fluxes) would be the first neutrinos which could be detected. Figure 8, left side (green curve) shows the contribution of solar neutrinos to the electronic recoil spectrum of XENON1T.

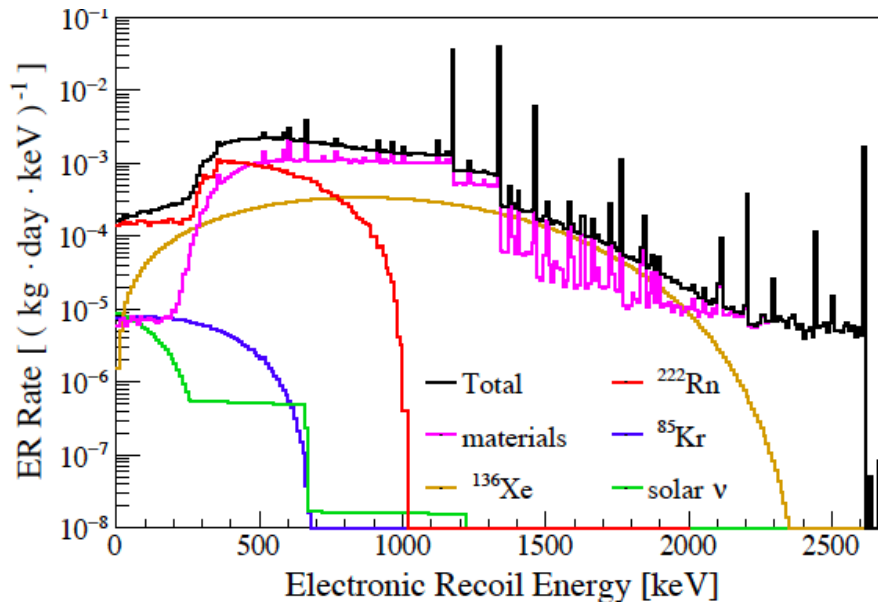


Figure 8. Contributions of different background sources to the ER region for XENON1T. Figure from [10].

Additionally, neutrinos can interact with the nucleus, in a similar way as dark matter, via coherent neutrino-nucleus scattering (we will discuss this process in a dedicated lecture). This process would induce nuclear recoils with energies up to few keV [11]. This process has been measured for the first time only in 2017 by the COHERENT collaboration [12]. The contribution of different neutrino sources to the nuclear recoil background of XENON1T is shown in figure 9. Coherent scattering of solar neutrinos (${}^8\text{B}$ and hep in blue and pink, respectively) would limit the sensitivity of dark matter experiment for low WIMP masses (few GeV). For higher masses, atmospheric neutrinos (in green) would limit dark matter searches [13].

Internal and surface backgrounds

Crystalline detectors: typically contamination of the crystal matrix with radioactive isotopes is negligible. The targets are grown from high purity powders or melts, and impurities are expelled during the crystallization process. The most important background for these detectors are surface contaminations. Either α -, β -decays or

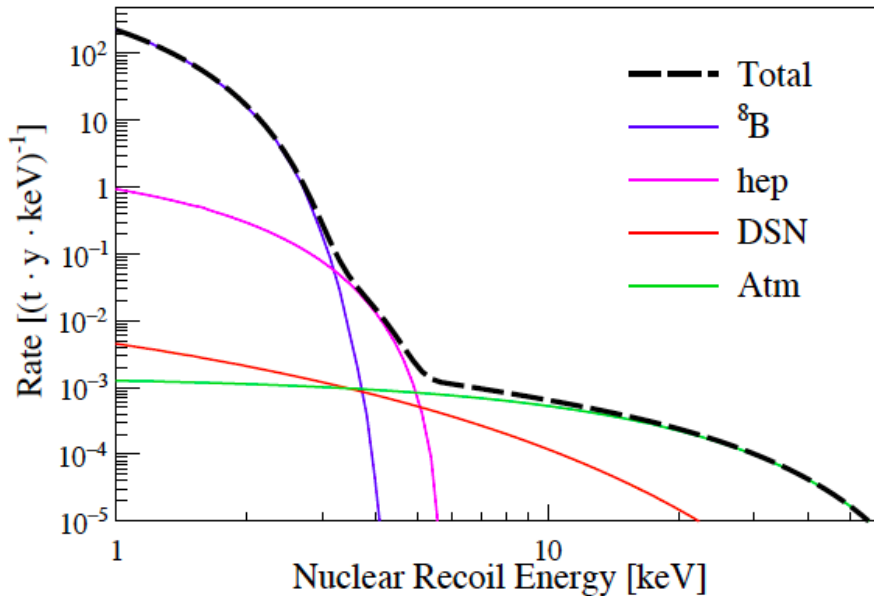


Figure 9. Spectral shape of coherent neutrino scattering in xenon. Figure from [10].

the nuclear recoils associated to the latter can enter the crystal depositing part of its energy. In addition, cosmic activation of the target or detector surrounding materials can contribute. Spallation of nuclei by high energy protons and neutrons can create long-lived isotopes. To avoid activation, transportation via airplane is avoided and the time the materials spend at surface is minimized.

Noble gas detectors: internal background arising from cosmogenic-activated or long-lived radioactive isotopes contained in the target nuclei.

- Argon: ^{39}Ar with an endpoint energy at 565 keV is contained in natural argon at a level of 1 Bq/kg. As this isotope is cosmogenically activated, reduction is possible by employing argon from underground reservoirs.
- Xenon: cosmic activation produces rather short-lived isotopes. However, xenon also contains a double beta decaying isotope: ^{136}Xe . Its lifetime is so large, 2.2×10^{21} y, that it doesn't contribute to the background for detectors up to few tons mass. ^{124}Xe is also contained in natural xenon. It decays via double electron capture and has a half-life of 1.8×10^{22} y, the longest half-life ever measure directly.

In addition the target can be contaminated with other noble gases as krypton or radon emanated from the detector materials.

- ^{85}Kr : β -decaying isotope produced in nuclear fission. It is released to the atmosphere by nuclear-fuel reprocessing plants and in nuclear weapons tests. It is present in atmospheric argon and krypton. Krypton can be removed from xenon either by cryogenic distillation or using chromatographic separation. See blue curve in figure 8.

- Radon is emanated from all detector materials containing traces of uranium or thorium and it is dissolved in the liquid target. See red curve in figure 8. An approach to reduce radon is to use materials with low radon emanation. Furthermore, distillation or adsorption can be employed to continuously remove the emanated radon.

1.5. Statistical treatment of data

The net result of a dark matter experiment is (eventually) a small number of signal events and a number of background events. Generally, direct dark matter detectors aim to a very low background such that the significance of event just a few signal events is high.

Given the fact that both signal and background number of events are expected to be low, special care has to be taken when extracting conclusions on the presence of a signal in the data. The counting method was commonly used in the past. It is also called Feldman and Cousins method [14] and takes into account the signal, the background and their corresponding fluctuations. This construction is used to derive both two-sided confidence intervals and upper confidence limits. Figure 10 (left) illustrates how this method can be applied. In a preselected window with large signal over background ratio, the background is estimated beforehand. From the number of events detected, the significance of the signal can be derived. The Feldman & Cousins method however

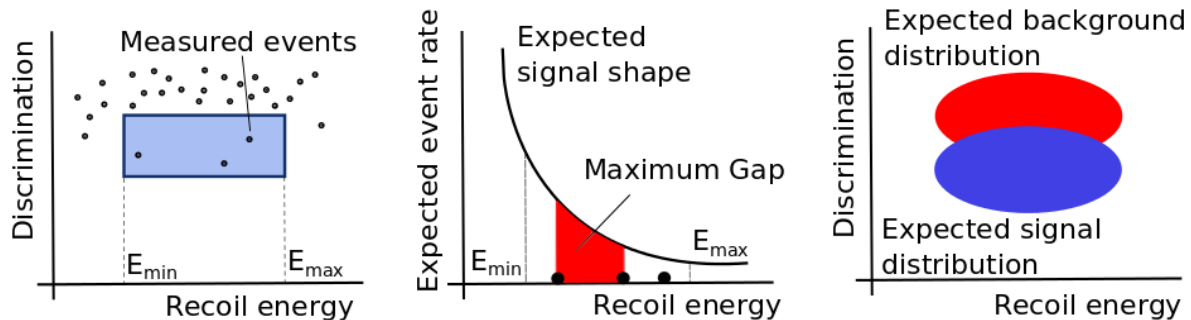


Figure 10. Illustration of different statistical methods used to derive results from direct detection experiments. Figure from [6].

does not take into account any information on the spectral shape of background or signal.

Another method being used is the maximum gap or optimum interval method (also called Yellin's method [15]). In this case, the shape of the expected signal is taken into account but does not make any assumption on the background. It is used when there is no knowledge (or poor knowledge) about the background level. It allows to derive a result (always a limit) even in cases where the background is unknown but it has the disadvantage that it can be used only to set upper limits (figure 10 middle).

The most common method is the maximum likelihood. It is used when it is possible to determine the probability density function (pdf) of both signal and background(s). Typically two hypotheses are tested: background only and background + signal hypothesis. For experiments that cannot separate between electronic recoils and nuclear recoils, a 1-dimensional pdf (energy dependence) of signal and background is employed. While for experiments that can separate those, a 2-dimensional pdf (energy and separation/discrimination parameters) are considered.

1.6. Detector calibration

An important topic is all experiments but specially in dark matter (due to the low energies) is the conversion from phonons, photons or charge to an actual recoil energy (keV_{nr}). There are different methods to determine the conversion to recoil energy: neutron scattering experiments, MC/data comparisons and modelling of underlying processes.

Neutron scattering experiments are the most direct method. A mono energetic neutron source, a detector with the medium of interest and a coincidence detector are positioned as in figure 11. In this figure the medium is marked as liquid xenon (LXe) but the same can be applied for a germanium, a NaI or any other detector medium. For fixed kinematics (positions and neutron energy), the nuclear recoil energy is also fixed.

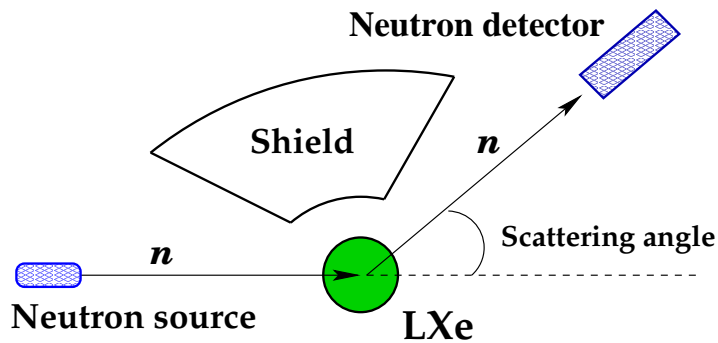


Figure 11. Schematic of a neutron scattering experiment. From [6].

In addition, for experiments with separation capabilities between electronic- and nuclear recoils, the corresponding regions need to be determined.

1.7. Technologies and results

The energy deposition from a WIMP-induced interaction results in a measurable signal which depends on the technology used. Phonons are produced in crystals, photons in scintillators and charges in ionization detectors. While one of these signals can be employed to reconstruct the energy of the recoil, the addition of another signal allows to distinguish between different types of particles. Figure 12 show a diagram with assigning each detector technology, the quanta that can be measured. The technologies

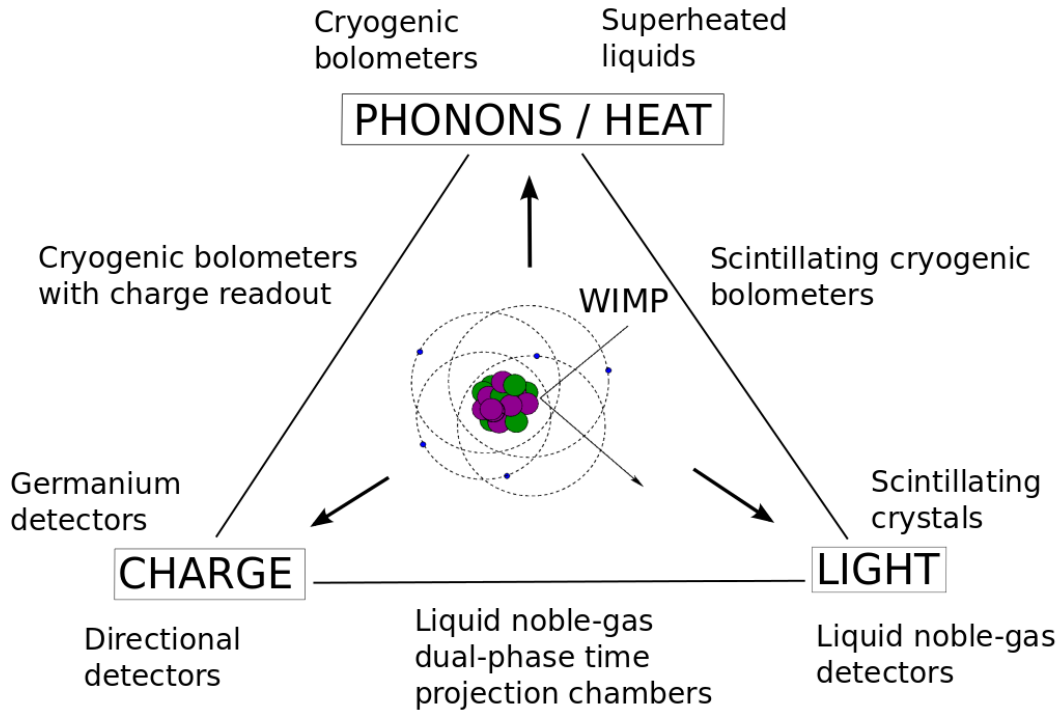


Figure 12. Schematic of signals in different detection technologies. Figure from [6].

in-between two categories, for instance scintillating cryogenic bolometers, combine these two measurements (e.g. light and phonons). This section described most of the technologies that can be used for direct detection of dark matter.

1.7.1. Scintillation detectors In these detectors, the energy deposition by charged particles produce excitation of the medium which de-excites via photon emission. Mostly NaI (Tl) and CsI (Tl) are used in dark matter searches. Advantages of this technology are the high density and large light output. Additionally, it is a 'simple' technology (good for long term stability) and low backgrounds can be achieved as the crystal are very pure. Arrays of several cm^3 crystals are however necessary to achieve large target masses. An important disadvantage is also that no electronic/nuclear recoil discrimination can be achieved. As a consequence the annual modulation signature is used.

DAMA is an important experiment being operated at LNGS laboratory in Italy. An annual modulating signal is present in the data, which has been taken over 20 annual cycles, at $\sim 13\sigma$ significance in an exposure of $2.46 \text{ ton}\cdot\text{y}$ [16]. The signal is in the $(1 - 6) \text{ keV}$ energy range with the maximum compatible with expectation (June 2nd) within 2σ . Figure 13 shows the data as released in 2008 (that time with a threshold of 2 keV).

Many other experiments cannot confirm (or have excluded) most of the dark

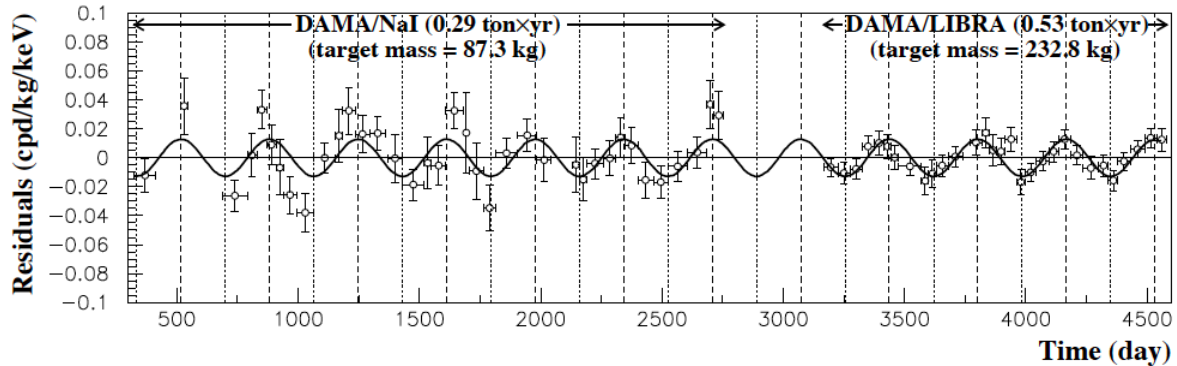


Figure 13. Residual rate of single-hit scintillation events by the DAMA/LIBRA experiment in the (2 – 6) keV energy region as a function of time. Figure from the DAMA coll. Eur. Phys. J. C56 (2008) 333, arXiv:0804.2741.

matter interpretations of the DAMA signal. Therefore, the origin of the signal remains unclear/controversial. Other non-dark matter related explanations of the DAMA signal: atmospheric muons (annually modulated due to temperature variations in the stratosphere, combinations of muons and modulated neutrinos (caused by the varying Sun-Earth distance) or varying rates of background neutrons have been considered.

1.7.2. Cryogenic bolometers These detectors have a very good energy resolution and an ultra-low threshold. For this reason, they are currently targeted to measure low mass WIMPs. The separation of signal and background is performed by combining phonon/charge and phonon/light signals. As for the scintillators in the previous section, scalability is not easy. Each crystal has ~ 1 kg and therefore several are necessary to achieve large masses.

Working principle: an energy deposition by a charged particle recoil is dissipated via collisions with the nuclei and electrons in the crystal lattice. Phonons are produced in this process. A bolometer measures an increase of temperature which is related to the heat capacity of the crystal. The signal has an exponential decay shape related to the thermal conductance of the thermal link (see figure 14 left) As an example: for a germanium detector at 20 mK, a few keV_{nr} would produce approx. $1 \mu\text{K}$ temperature difference. To detect this tiny temperature increase, the thermal bath is typically at a temperature of (10 – 100) mK.

The phonon signal can be combined with either a charge or a scintillation signal. Germanium or silicon detectors can record the combination of phonon and charge read-out. They have a very good particle separation (see red and blue populations in figure 14 right). SuperCDMS [17] and Edelweiss [18] (see figure 16) are examples of such detectors. If instead scintillating bolometers are employed (as in CaWO_4 detectors), light and phonons can be recorded. CRESST is an example of an experiment using this technology which has the best sensitivity at low WIMP masses [19] (see also figure 20).

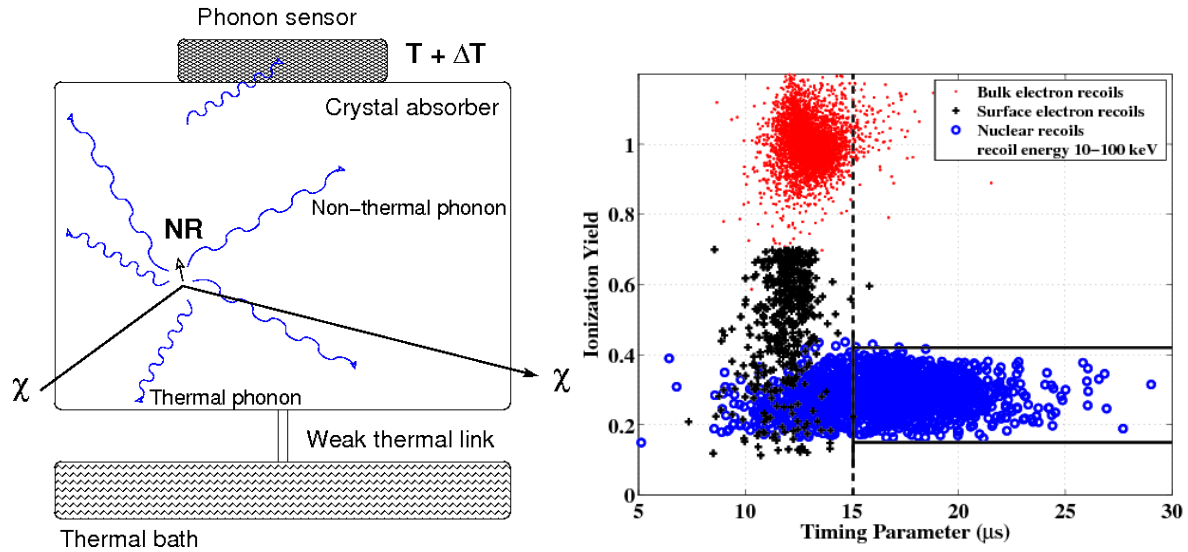


Figure 14. Left: Schematic representation of a cryogenic bolometer. Right: Ionisation yield and timing parameter for electronic recoils, nuclear recoils and surface events. Figure from CDMS Coll., Phys. Rev. Lett. 102 (2009) 011301.

1.7.3. Liquid noble-gas detectors This technology is currently the most successful one meaning that the best sensitivities for dark matter coupling to ordinary matter are obtained. It has the major advantage of reaching in a rather easy way large masses and homogeneous targets. Using the scintillation light and the charge signals, a 3D position reconstruction of the event can be performed.

Working principle: the energy deposition from a nuclear recoil excites (R^*) and ionizes (R^+) the medium. Excited dimers are formed which decay emitting light: $R^* + R \rightarrow R_2^*$ followed by $R_2^* \rightarrow 2R + h\nu$. The scintillation light $h\nu$ appears with two time constants: 5 ns/1.6 μs and 3 ns/30 ns for liquid argon (LAr) and liquid xenon (LXe), respectively. Free electrons are produced in the ionization process. Without an applied electric field, all charges recombine giving additional scintillation light. However, if the medium is placed in an electric field, part of the charges (e^-) are extracted and cannot recombine (less light) but an additional signal can be read out. There are in principle two types of noble gas detectors: single phase is only light is read-out and double-phase (with a gas phase on top) to record also the charge signal.

Single phase detectors consist of a liquid volume (typically a sphere) surrounded by photosensors (see figure 15). Due to the good photosensor coverage (4π), a very good light collection results. Particle separation (ER from NRs) is possible through pulse shape differences as the amplitudes of the singlet and triplet components depend on the particle type. DEAP [20] (LAr, see figure 16) at SNOLAB in Canada and XMASS [21] (LXe) at Kamioka in Japan are example of single-phase liquid noble gas detectors.

In double-phase TPCs, both the scintillation light and charges are detected. The scintillation light is recorded in two arrays of photomultipliers on top and bottom of

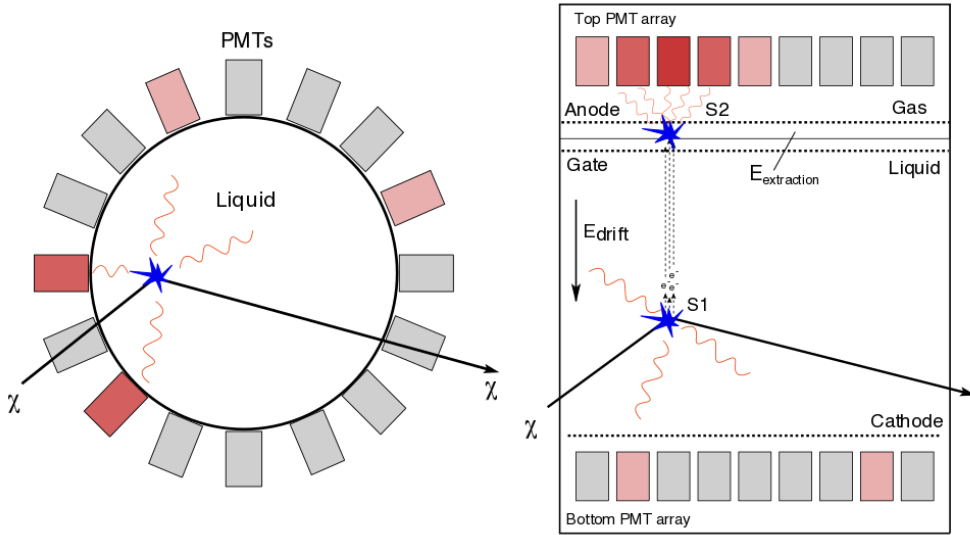


Figure 15. Schematic of single-phase (left) and double-phase (right) liquid noble-gas detectors.

the cylindrical shaped cage. Charges are extracted from the interaction point with an electric drift field. These charges are amplified and converted to light in the gas phase. XENON1T [22] (see figure 16) at LNGS in Italy, PandaX at Jin-Ping in China [23] and LUX at Sanford in the US [24] are examples of LXe TPCs. Dark-Side is an example of a LAr TPC [25] located also at LNGS. As shown in figure 20 liquid xenon TPCs have most sensitive constrains on the cross section to ordinary matter for WIMP masses above $\sim 5 \text{ GeV}/c^2$.

[Exercise related to XENON](#)

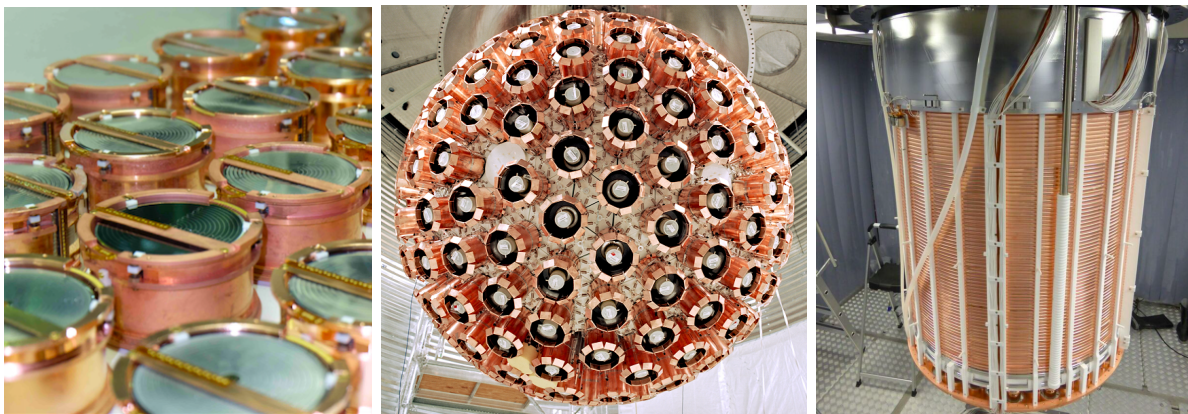


Figure 16. Photographs of different direct detection experiments. The Edelweiss cryogenic bolometer (left), the DEAP single phase liquid argon detector and the double-phase TPC XENON1T. Figures from the corresponding collaboration homepages.

1.7.4. *Bubble chambers* Bubble chambers were often used in the last decades in accelerator experiments until new technologies provided a better performance (as gaseous detectors). This technology has been revived in the context of dark matter searches over the last years.

Working principle: the medium is a superheated liquid below the boiling point. Charged particles create ionization/heat that result into bubble formation. When the bubbles grow, they can be photographed with CCD cameras. Figure 17 shows three photographs of events: a muon on the left, a multiple scattering likely from a neutron (middle) and a single scattering on the right as expected from dark matter interactions.

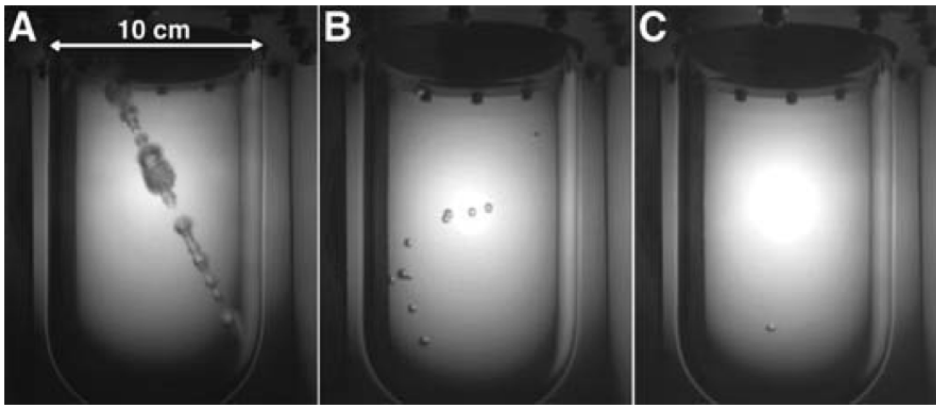


Figure 17. Events in a superheated-liquid bubble chamber (1.5 kg of CF_3I). A: muon track, B: nuclear recoils from neutrons, C: expected signature of a WIMP interaction, a single nuclear recoil bubble. Figure from COUPP Coll., *Science* 319 (2008) 933, arXiv:0804.2886.

An advantage of these detectors is that they can be tuned to be sensitive only to high dE/dx particles. In this way, background from e^- , γ , β and muons are avoided and a low overall background level can be reached. α -particles do in principle contribute to the background. This contribution can be reduced using the acoustic signal as interestingly, the sound of an alpha particle is different from the sound of a nuclear recoil. Figure 18 shows an example of the separation power of the acoustic parameter (AP). In addition, they have a very good sensitivity to spin-dependent interactions. Fluorine is used in the target and has a particular large expectation value for the proton spin content which enhances the sensitivity for spin dependent interactions to protons. After the bubble formation, the medium needs to be recompressed resulting into a certain dead-time for the experiment. The current best results on spin-dependent proton coupling is from the PICO experiment which employs this technology [26].

1.7.5. *Directional searches* As discussed in section 1.1, a strong directional dependence of the signal is expected. The range of a WIMP-induced nuclear recoil in solids/liquids is < 100 nm for $E_{th} < 200$ keV. Therefore, mainly low pressure gas TPCs (< 130 mbar) are

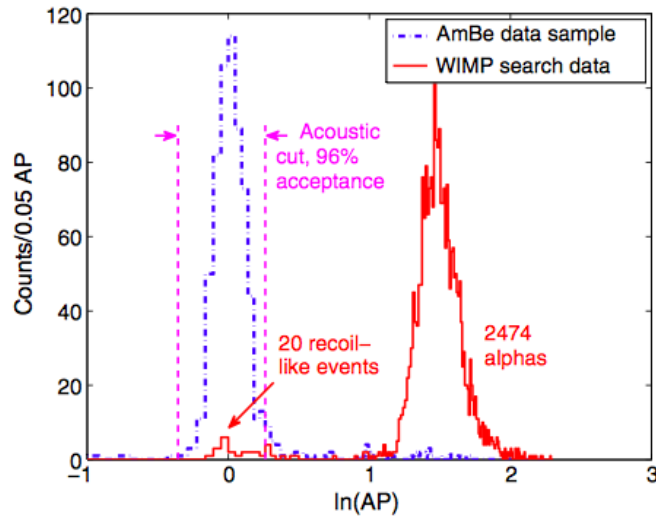


Figure 18. Distribution of nuclear recoils (blue) and alpha events (red) in an acoustic parameter (AP) in the COUPP experiment. Figure from COUPP Coll., Phys. Rev. D 86 (2012) 052001.

employed for this kind of searches. A $100 \text{ GeV}/c^2$ WIMP mass with 220 km/s velocity can produce a recoil track of $1\text{-}2 \text{ mm}$ in such low pressure gas.

Although this would be a very clear dark matter signature, the disadvantage is the low sensitivity. Low pressure means low density and this implies a low target mass. For this reason, 'huge' detectors are necessary to be competitive. Another difficulty is the diffusion of the charges when they drift through the medium. This leads to a loss of directional sensitivity. Figure 19 shows a scheme of a low pressure directional detector. The DRIFT-II experiment [27] running at the Boulby mine in the UK is an example of

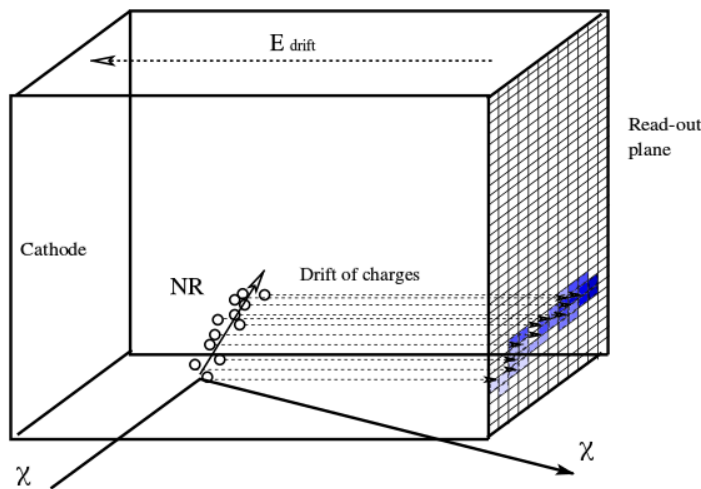


Figure 19. Schematic of a track reconstruction in a directional low-pressure gaseous time-projection chamber (TPC). Figure from [6].

a low pressure directional detector. The last result from this experiment is the most sensitive for directional searches but it is not yet competitive with other searches.

1.8. Summary

In this lecture we summarized the principles of direct detection: signal properties, backgrounds and treatment of data. We discussed also most of the existing technologies including their advantages and disadvantages. As no conclusive evidence for dark matter has appear in the data yet, the race continues.

Figure 20 shows an overview of direct detection results for spin-independent WIMP-nucleon cross sections. The shaded green region represents the region in parameter space which is excluded by current experiments. The orange shaded region represent the neutrino floor: the cross sections at which coherent neutrino scattering is an irreducible background.

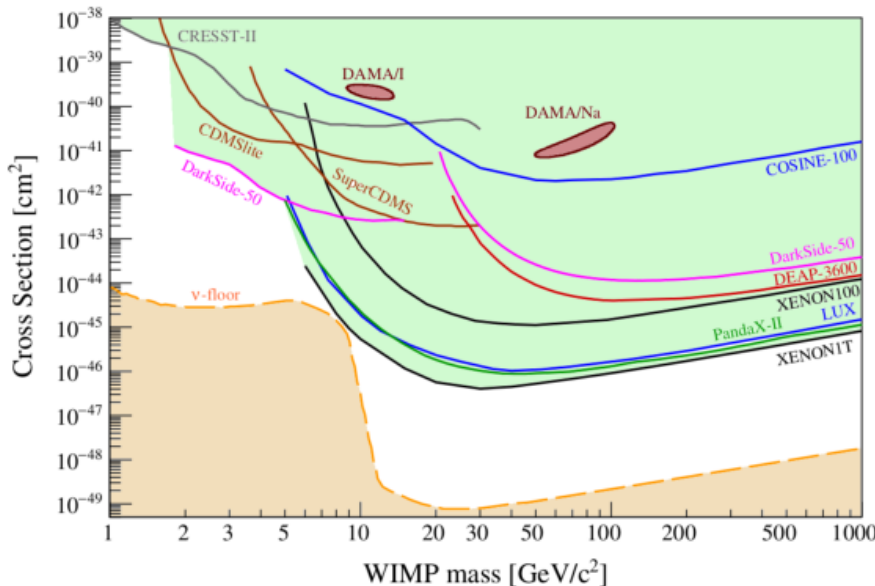


Figure 20. Spin-independent direct detection results. Figure from [28].

References

- [1] J. Lewin and P. Smith, “Review of mathematics, numerical factors, and corrections for dark matter experiments based on elastic nuclear recoil,” *Astropart. Phys.* **6** (1996) 87.
- [2] A. Drukier, K. Freese, and D. Spergel, “Detecting Cold Dark Matter Candidates,” *Phys. Rev. D* **33** (1986) 3495.
- [3] K. Freese, M. Lisanti, and C. Savage, “Colloquium: Annual modulation of dark matter,” *Rev. Mod. Phys.* **85** (2013) 1561, [arXiv:1209.3339](https://arxiv.org/abs/1209.3339).
- [4] D. N. Spergel, “The Motion of the Earth and the Detection of Weakly interacting massive particles,” *Phys. Rev. D* **37** (1988) 1353.

- [5] R. H. Helm, “Inelastic and Elastic Scattering of 187-MeV Electrons from Selected Even-Even Nuclei,” *Phys. Rev.* **104** (1956) 1466.
- [6] T. Marrodán Undagoitia and L. Rauch, “Dark matter direct-detection experiments,” *J. Phys.* **G43** no. 1, (2016) 013001, [arXiv:1509.08767](#).
- [7] W. R. Leo, *Techniques for Nuclear and Particle Physics Experiments*. Springer-Verlag, Berlin, Heidelberg, Second revised edition, 1994.
- [8] G. Heusser, M. Weber, *et al.*, “GIOVE - A new detector setup for high sensitivity germanium spectroscopy at shallow depth,” *Eur. Phys. J. C* **75** no. 11, (2015) 531, [arXiv:1507.03319](#).
- [9] B. Cabrera, L. M. Krauss, and F. Wilczek, “Bolometric Detection of Neutrinos,” *Phys. Rev. Lett.* **55** (1985) 25.
- [10] **XENON** Collaboration, E. Aprile *et al.*, “Physics reach of the XENON1T dark matter experiment,” *JCAP* **04** (2016) 027, [arXiv:1512.07501](#).
- [11] D. Z. Freedman, “Coherent neutrino nucleus scattering as a probe of the weak neutral current,” *Phys. Rev.* **D9** (1974) 1389.
- [12] **COHERENT** Collaboration, D. Akimov *et al.*, “Observation of Coherent Elastic Neutrino-Nucleus Scattering,” *Science* **357** no. 6356, (2017) 1123, [arXiv:1708.01294](#).
- [13] L. E. Strigari, “Neutrino Coherent Scattering Rates at Direct Dark Matter Detectors,” *New J. Phys.* **11** (2009) 105011, [arXiv:0903.3630](#).
- [14] G. J. Feldman and R. D. Cousins, “A Unified approach to the classical statistical analysis of small signals,” *Phys. Rev.* **D57** (1998) 3873, [arXiv:physics/9711021](#).
- [15] S. Yellin, “Finding an upper limit in the presence of unknown background,” *Phys. Rev.* **D66** (2002) 032005, [arXiv:physics/0203002](#).
- [16] R. Bernabei *et al.*, “First model independent results from DAMA/LIBRA-phase2,” *Nucl. Phys. Atom. Energy* **19** no. 4, (2018) 307, [arXiv:1805.10486](#).
- [17] **SuperCDMS** Collaboration, R. Agnese *et al.*, “Search for Low-Mass Weakly Interacting Massive Particles with SuperCDMS,” *Phys. Rev. Lett.* **112** (2014) 241302, [arXiv:1402.7137](#).
- [18] **EDELWEISS** Collaboration, E. Armengaud *et al.*, “Performance of the EDELWEISS-III experiment for direct dark matter searches,” *JINST* **12** no. 08, (2017) P08010, [arXiv:1706.01070](#).
- [19] **CRESST** Collaboration, G. Angloher *et al.*, “Results on light dark matter particles with a low-threshold CRESST-II detector,” [arXiv:1509.01515](#).
- [20] **DEAP** Collaboration, M. Boulay, “DEAP-3600 Dark Matter Search at SNOLAB,” *J. Phys. Conf. Ser.* **375** (2012) 012027, [arXiv:1203.0604](#).
- [21] K. Abe *et al.*, “XMASS detector,” *Nucl. Instrum. Meth.* **A716** (2013) 78, [arXiv:1301.2815](#).
- [22] **XENON** Collaboration, E. Aprile *et al.*, “Dark Matter Search Results from a One Ton-Year Exposure of XENON1T,” *Phys. Rev. Lett.* **121** no. 11, (2018) 111302, [arXiv:1805.12562](#).
- [23] **PandaX-II** Collaboration, X. Cui *et al.*, “Dark Matter Results From 54-Ton-Day Exposure of PandaX-II Experiment,” *Phys. Rev. Lett.* **119** no. 18, (2017) 181302, [arXiv:1708.06917](#).
- [24] **LUX** Collaboration, D. Akerib *et al.*, “Results from a search for dark matter in the complete LUX exposure,” *Phys. Rev. Lett.* **118** no. 2, (2017) 021303, [arXiv:1608.07648](#).
- [25] **DarkSide** Collaboration, P. Agnes *et al.*, “DarkSide-50 532-day Dark Matter Search with Low-Radioactivity Argon,” *Phys. Rev. D* **98** no. 10, (2018) 102006, [arXiv:1802.07198](#).
- [26] **PICO** Collaboration, C. Amole *et al.*, “Dark Matter Search Results from the Complete Exposure of the PICO-60 C₃F₈ Bubble Chamber,” *Phys. Rev. D* **100** no. 2, (2019) 022001, [arXiv:1902.04031](#).
- [27] **DRIFT** Collaboration, J. Battat *et al.*, “First background-free limit from a directional dark matter experiment: results from a fully fiducialised DRIFT detector,” [arXiv:1410.7821](#).
- [28] M. Schumann, “Direct Detection of WIMP Dark Matter: Concepts and Status,” *J. Phys. G* **46** no. 10, (2019) 103003, [arXiv:1903.03026](#).